



Effect of calcination temperature on morphology and electrochemical performance of $\text{PbLi}_2\text{Ti}_6\text{O}_{14}$

Jundong Zhang¹, Haoxiang Yu¹, Nengbing Long*, Tingting Liu, Xing Cheng, Runtian Zheng, Haojie Zhu, Wuquan Ye, Jie Shu*

School of Materials Science and Chemical Engineering, Ningbo University, Ningbo 315211, China

ARTICLE INFO

Keywords:

$\text{PbLi}_2\text{Ti}_6\text{O}_{14}$
Electrochemical behavior
Lithium ion batteries
In-situ observation
Anode material

ABSTRACT

As a promising anode material, $\text{PbLi}_2\text{Ti}_6\text{O}_{14}$ has attracted the attention of many researchers. In this work, a series of $\text{PbLi}_2\text{Ti}_6\text{O}_{14}$ are prepared by solid state method at five different calcination temperatures and used as anode materials in lithium ion batteries. Through a series of tests, the results show that the phase purity, morphology and electrochemical performance of $\text{PbLi}_2\text{Ti}_6\text{O}_{14}$ can be seriously influenced by calcination temperature. When the calcination temperature is 900 °C, the phase-pure $\text{PbLi}_2\text{Ti}_6\text{O}_{14}$ can be obtained with relatively small particle size, excellent cycle performance and outstanding lithium ion diffusion behavior. It provides an initial charge capacity of 151.3 mA h g^{-1} at 100 mA g^{-1} . After 100 cycles, it shows a reversible capacity of 142.0 mA h g^{-1} with superior capacity retention of 93.85%. In contrast, $\text{PbLi}_2\text{Ti}_6\text{O}_{14}$ formed at 800 °C displays an unsatisfactory performance due to the presence of impurity, even though it has the smallest particle size and the largest lithium ion diffusion coefficient among the five samples. The reversible capacity is only 82.6 mA h g^{-1} after 100 cycles with capacity retention of 53.9%. In order to further study the lithium ion diffusion behavior of $\text{PbLi}_2\text{Ti}_6\text{O}_{14}$, the in-situ X-ray diffraction technique is also implemented. It is found that during the lithiation/delithiation process, the stable framework can effectively inhibit the volume change and ensures the excellent electrochemical performance of $\text{PbLi}_2\text{Ti}_6\text{O}_{14}$.

1. Introduction

Excessive use of fossil fuels has accelerated the depletion of the earth energy. As an energy storage and conversion devices, rechargeable lithium ion batteries (LIBs) play a significant role in solving the existing problems of energy depletion and environmental pollution. Now, LIBs have been widely used in people's production and life [1,2]. The demand for outstanding LIBs in various portable electronic devices continues to grow. However, most of the current LIBs use graphite, soft carbon, hard carbon and other single intercalated lithium carbon materials as anode materials. These carbonaceous materials exhibit high capacities but with poor rate performance. During the past few years, numerous efforts have been made to develop new anode materials with high capacity and super cycle stability to replace carbonaceous materials.

Recently, titanates occupy an important position among multitudinous explored materials [3]. As a well-known anode material, $\text{Li}_4\text{Ti}_5\text{O}_{12}$ has obtained comprehensive attention due to its stable structure and exceptional electrochemical performance [4,5]. Since a

new phase composed of Sr, Li and Ti was discovered from the $\text{SrO-TiO}_2\text{-LiBO}_2$ system by Koseva in 1991 [6]. Various types of titanate materials have been noted as the high voltage anode materials. The single crystal of $\text{SrLi}_2\text{Ti}_6\text{O}_{14}$ has been grown by the flux method and its structure was determined in 2002 [7]. A novel family of isostructural titanates $\text{MLi}_2\text{Ti}_6\text{O}_{14}$ ($\text{M} = \text{Ba, Sr, Pb}$) was reported by Koseva, which can be one of promising materials to replace graphitic anodes in LIBs [8]. According to the previous literature reported by Dambournet, the electrochemical performance of $\text{SrLi}_2\text{Ti}_6\text{O}_{14}$ is superior to those of $\text{BaLi}_2\text{Ti}_6\text{O}_{14}$ and $\text{Na}_2\text{Li}_2\text{Ti}_6\text{O}_{14}$ under the same conditions [9].

As a member of titanates family, $\text{PbLi}_2\text{Ti}_6\text{O}_{14}$ also exhibits excellent electrochemical performance. Li ever reported the electrochemical performance of $\text{PbLi}_2\text{Ti}_6\text{O}_{14}$ obtained from solid state preparation. It suggests that $\text{PbLi}_2\text{Ti}_6\text{O}_{14}$ can express remarkable cyclability and rate performance. After 1000 cycles, $\text{PbLi}_2\text{Ti}_6\text{O}_{14}$ only shows 12.5% capacity fading of the first cycle at 1000 mA g^{-1} [10]. However, they did not detail the impact of calcination temperature on the morphology and electrochemical properties of $\text{PbLi}_2\text{Ti}_6\text{O}_{14}$. Therefore, further investigation on the influence of calcination temperature for $\text{PbLi}_2\text{Ti}_6\text{O}_{14}$

* Corresponding authors.

E-mail addresses: longnengbing@nbu.edu.cn (N. Long), shujie@nbu.edu.cn (J. Shu).

¹ These authors contributed equally to this work.

<https://doi.org/10.1016/j.ceramint.2018.02.169>

Received 11 February 2018; Received in revised form 21 February 2018; Accepted 21 February 2018
0272-8842/ © 2018 Elsevier Ltd and Techna Group S.r.l. All rights reserved.

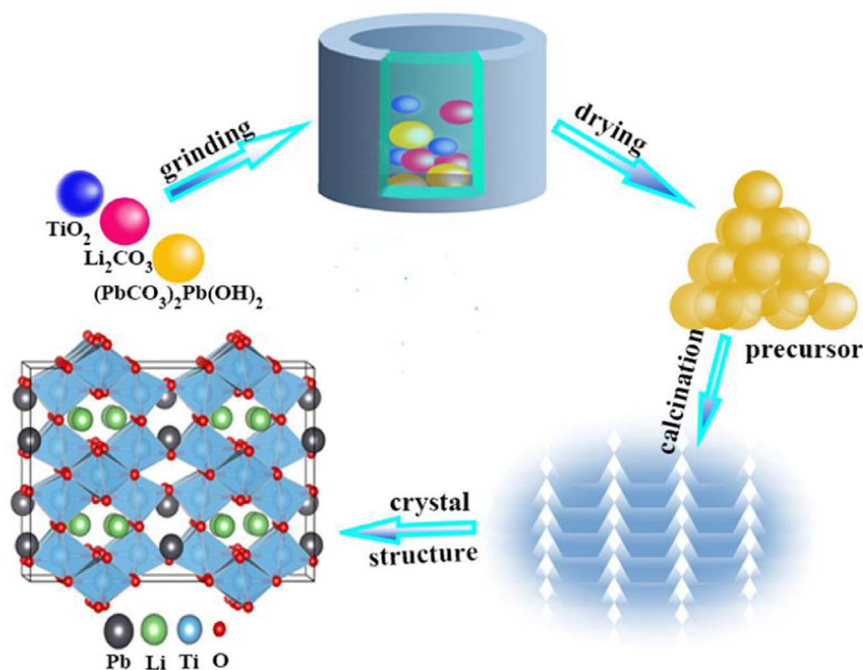


Fig. 1. Schematic illustration of the formation for $\text{PbLi}_2\text{Ti}_6\text{O}_{14}$.

still needs to be carried out. In this work, $\text{PbLi}_2\text{Ti}_6\text{O}_{14}$ is synthesized by the solid state methods at the various calcination temperatures ranged from 800 to 1000 °C. In order to elucidate the morphology, electrochemical performance and lithium storage behavior, a series of measurements are performed thoroughly. The optimum calcination temperature of $\text{PbLi}_2\text{Ti}_6\text{O}_{14}$ is finally determined.

2. Experimental

The schematic illustration of the formation of $\text{PbLi}_2\text{Ti}_6\text{O}_{14}$ via solid state reaction is illustrated in Fig. 1. The raw materials were Li_2CO_3 (Aladdin, 99.5%) $(\text{PbCO}_3)_2\text{Pb}(\text{OH})_2$ (Aladdin, 99.5%) and TiO_2 (Aladdin, 99.5%). They were mixed by ball milling in anhydrous ethanol for 12 h and the molar ratio of Li/Pb/Ti was 2.02:1:6. After that, the precursor was obtained. The precursor was dried in an oven at 80 °C and then calcined in a muffle furnace. The calcination was divided into two steps. In the first step, the precursor was pre-calcined at 600 °C for 4 h. In the second step, the powder obtained in the first step was subsequently calcined at 800, 850, 900, 950 and 1000 °C for 15 h, respectively. Finally, the target compounds were obtained. In the process of calcination, an excess of 2% Li salt was added in order to compensate for the loss of Li source under high temperature conditions. The structures of five samples were identified on a Bruker D8 Focus X-ray diffraction (XRD) instrument with Cu K α radiation from 10° to 50° in a sweep speed of 0.02° s⁻¹. The surface morphologies of samples were measured on a Hitachi S4800 scanning electron microscopy (SEM).

The electrochemical performances of the samples are evaluated in Swagelok-type cells with lithium disk as the counter electrode and Whatman glass fiber as separator. The working electrode was prepared by mixing the active material, acetylene black as conductive agent, and polyvinylidene fluoride as adhesive at a ratio of 8:1:1. Then, the homogenous slurry was cast onto copper foil and subsequently dried in a vacuum oven at 120 °C for 24 h. All the cells were assembled in a glovebox filled with argon. The electrolyte was a mixture which was obtained by 1 M LiPF_6 dissolved in EC-DMC (1:1, v/v, EC was ethylene

carbonate and DMC was methyl carbonate).

The charge/discharge cycles were tested on the Wuhan Land battery test system with operating voltage range of 0.5–2.0 V. Cyclic voltammetry (CV) test was measured by CHI1000B electrochemical workstation from 0.5 to 2.0 V at a scan rate of 0.1 mVs⁻¹. The electrochemical impedance spectroscopy experiment was carried out by CHI660D electrochemical workstation. The working frequency range was 10⁻²–10⁵ Hz.

3. Results and discussion

Fig. 2 demonstrates XRD patterns of samples which were

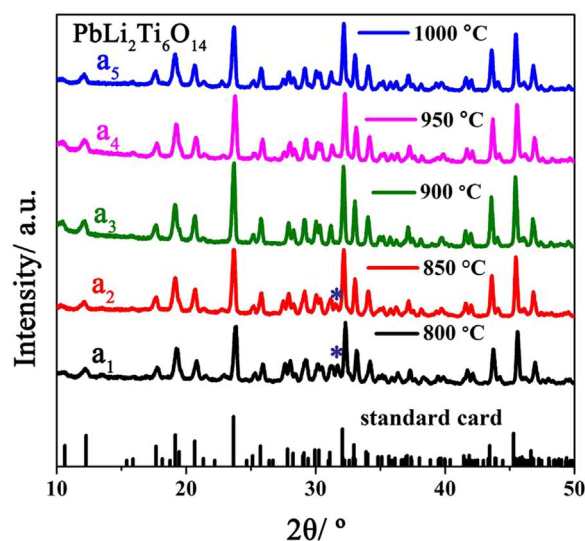


Fig. 2. XRD patterns of $\text{PbLi}_2\text{Ti}_6\text{O}_{14}$ at different temperature. (a₁) 800 °C, (a₂) 850 °C, (a₃) 900 °C, (a₄) 950 °C, (a₅) 1000 °C.

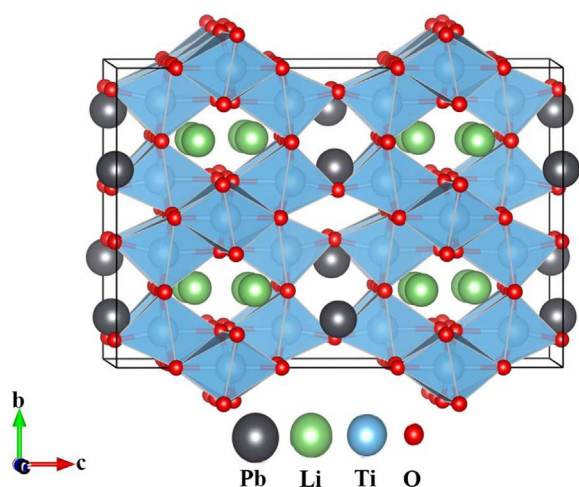


Fig. 3. Crystal structure of $\text{PbLi}_2\text{Ti}_6\text{O}_{14}$.

synthesized at five different calcination temperatures. When calcination temperatures are 800 and 850 °C, a trace amount of TiO_2 can be observed, suggesting that the solid-phase reaction does not go to

completion [11]. With the temperature increasing, impurity phases such as TiO_2 or Pb-containing compounds cannot find in the XRD patterns of $\text{PbLi}_2\text{Ti}_6\text{O}_{14}$. It suggests that $\text{PbLi}_2\text{Ti}_6\text{O}_{14}$ can be formed when the calcination temperature reaches 900 °C or above.

From the crystal structure of $\text{PbLi}_2\text{Ti}_6\text{O}_{14}$ in Fig. 3, it is easy to observe that the Ti-O octahedron is a skeleton structure of $\text{PbLi}_2\text{Ti}_6\text{O}_{14}$ and supports the entire crystal [12]. The environment around Ti atom is extremely complex. It occupies four different lattice locations. Li atom is in the gap of the Ti-O octahedron, and the Li-O tetrahedron is formed by the Li atom and the surrounding O atoms [13]. The Pb atom locates between two consecutive Ti-O octahedrons and forms Pb-O 11-coordinated polyhedron with the surrounding eleven O atoms. These structures make $\text{PbLi}_2\text{Ti}_6\text{O}_{14}$ have excellent lithium storage behavior.

Fig. 4 shows the SEM images of $\text{PbLi}_2\text{Ti}_6\text{O}_{14}$ at different calcination temperatures. The size of the particle becomes larger as the temperature increases. Fig. 4a-b displays the SEM images of $\text{PbLi}_2\text{Ti}_6\text{O}_{14}$ which is synthesized at 800 °C. The morphology of $\text{PbLi}_2\text{Ti}_6\text{O}_{14}$ particles presents a size distribution ranged from 200 to 500 nm, which is the smallest among these five samples. Similar phenomenon has found in the previous literature [14]. When the calcination temperature goes up to 850 °C as shown in Fig. 4c-d, the particle size of the sample is larger than $\text{PbLi}_2\text{Ti}_6\text{O}_{14}$ obtained at 800 °C. It is about 200–600 nm in size. With a further increase of calcining temperature to 900 °C, the resulting

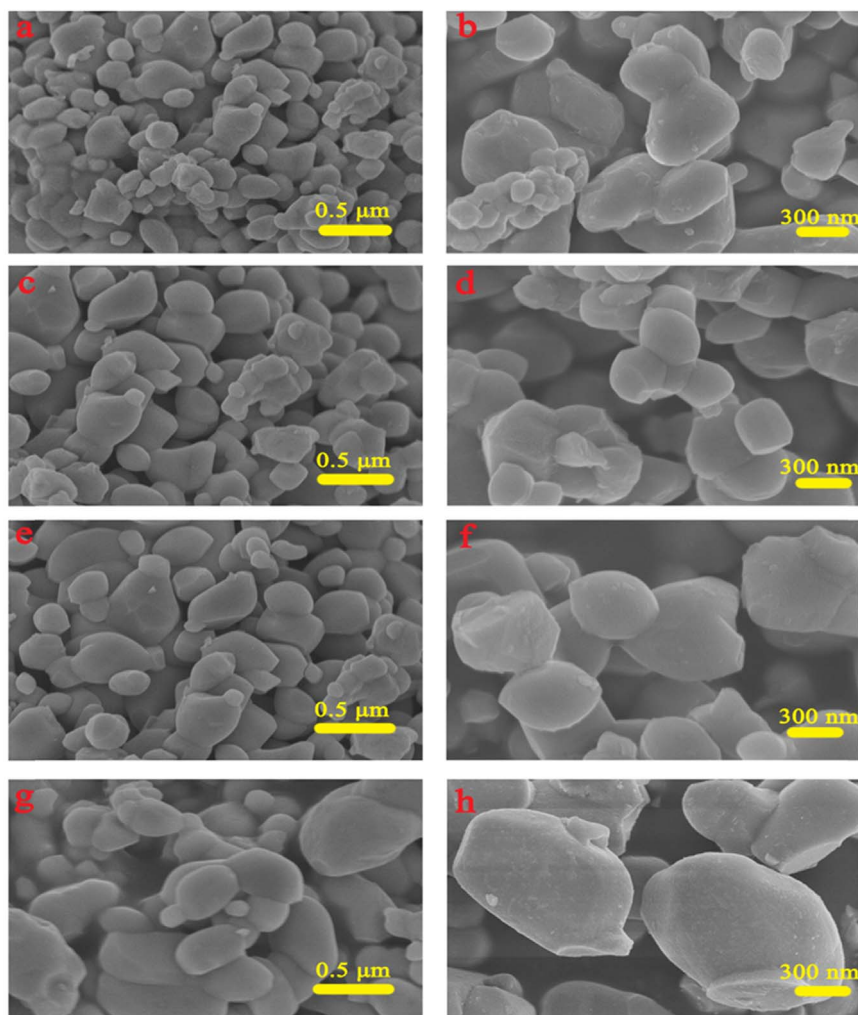


Fig. 4. SEM of $\text{PbLi}_2\text{Ti}_6\text{O}_{14}$ synthesized at different temperature. (a, b) 800 °C, (c, d) 850 °C, (e, f) 900 °C, (g) 950 °C, (h) 1000 °C.

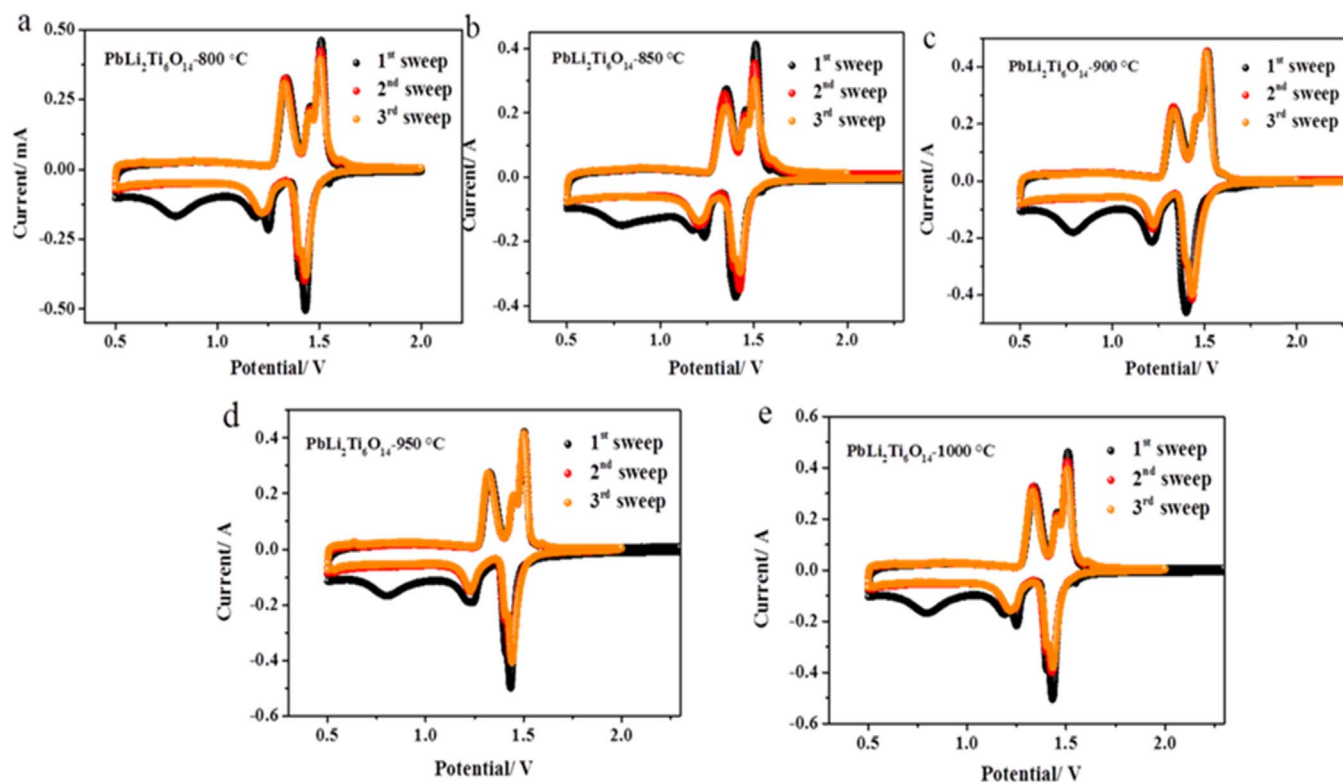


Fig. 5. Cyclic voltammograms of $\text{PbLi}_2\text{Ti}_6\text{O}_{14}$ synthesized at different temperature. (a) 800 °C, (b) 850 °C, (c) 900 °C, (d) 950 °C, (e) 1000 °C.

$\text{PbLi}_2\text{Ti}_6\text{O}_{14}$ particles show smooth surfaces with uniform sizes of 400–600 nm (Fig. 4e–f). As the temperatures rise up to 950 and 1000 °C, serious agglomeration can be observed in Fig. 4g–h. Meanwhile, the particle size is larger than $\text{PbLi}_2\text{Ti}_6\text{O}_{14}$ obtained at 900 °C. The results obtained from SEM show that the particle size of $\text{PbLi}_2\text{Ti}_6\text{O}_{14}$ can be influenced by calcination temperature. This result will affect the electrochemical properties of $\text{PbLi}_2\text{Ti}_6\text{O}_{14}$.

Fig. 5 shows CV curves for $\text{PbLi}_2\text{Ti}_6\text{O}_{14}$ yielded at various temperatures over a voltage range from 0.5 to 2 V. In order to make the experiment as accurate as possible, we ensure that the weight of the active substance on each working electrode is the same before performing the CV test [15,16]. No significant difference is found in the five CV diagrams except the current of peaks. The redox peaks appear at 1.51/1.43, 1.45/1.39 and 1.33/1.23 V, corresponding to voltage platforms of charge/discharge curves. From the first cycle of scan curve, a strong reduction peak is found at 0.79 V due to the decomposition of electrolyte. In Fig. 5a–b, a slight redox couple appears at 1.60/1.54 V, which is found to be due to the redox reaction of residual TiO_2 in the sample. However, this redox couple does not appear in Fig. 5c–e, indicating that there are no other phases formed in these samples [17]. This is consistent with the result obtained from XRD.

Fig. 6a–c depicts the 1st, 50th and 100th charge/discharge profiles of the samples synthesized at various temperatures cycled at 100 mA g^{-1} . Upon the initial cycle, three obvious voltage platforms can be found, matching well with the result obtained from CV curves. Simultaneously, the decomposition of electrolyte is also shown in the initial charge/discharge profiles. In Fig. 6a–c, an additional charge platform appears at 1.54 V in both of the charge/discharge profiles for $\text{PbLi}_2\text{Ti}_6\text{O}_{14}$ obtained at 800 and 850 °C. It proves the existence of TiO_2

[18]. In addition, the capacities of $\text{PbLi}_2\text{Ti}_6\text{O}_{14}$ obtained from 800° to 1000 °C are 153.3, 147.1, 151.3, 152.9 and $146.7 \text{ mA h g}^{-1}$, respectively, during the first cycle. After 50 cycles, the reversible capacities are 99.5, 135.5, 144.5, 129.8 and $123.3 \text{ mA h g}^{-1}$, respectively. It can be found that the sample obtained at 900 °C delivers the highest reversible capacity. After 100 cycles, the reversible capacities are 82.6, 130.0, 142.0, 121.8 and 86.6 mA h g^{-1} , respectively. The capacity of $\text{PbLi}_2\text{Ti}_6\text{O}_{14}$ obtained at 900 °C is still the highest one with capacity retention of 93.85%. The corresponding cyclic performances are shown in Fig. 6d. It is found that the high calcination temperature, especially for 1000 °C, results in the agglomeration of the $\text{PbLi}_2\text{Ti}_6\text{O}_{14}$ particles to form large particles, which affects the diffusion of lithium ions in the lattice of $\text{PbLi}_2\text{Ti}_6\text{O}_{14}$ and eventually have a bad effect on electrochemical properties [19–21]. All the results show that the best calcination temperature for the preparation of $\text{PbLi}_2\text{Ti}_6\text{O}_{14}$ is 900 °C. Fig. 6e shows the rate performance of $\text{PbLi}_2\text{Ti}_6\text{O}_{14}$ at current densities of $100\text{--}500 \text{ mA g}^{-1}$ for different calcination temperatures. The overall trend is consistent with the result in Fig. 6d. It is worth mentioning that the sample calcined at 900 °C also has the best rate performance among five samples.

Fig. 7a–d shows the results obtained from the EIS measurement. All the impedance curves are made by the flattened semicircle in the high frequency region and the slash in the low frequency region. As shown in Fig. 7a, The size of the semicircle represents the charge transfer resistance of LIBs at the interface of the electrolyte and the active material [22,23]. The slash represents a semi-infinite Warburg impedance process. The equivalent circuit diagram in Fig. 7b can intuitively reflect the internal impedance of the battery. R_s , R_{ct} , CPE and W denote solution resistance, charge transfer resistance, interface contact capacitance and

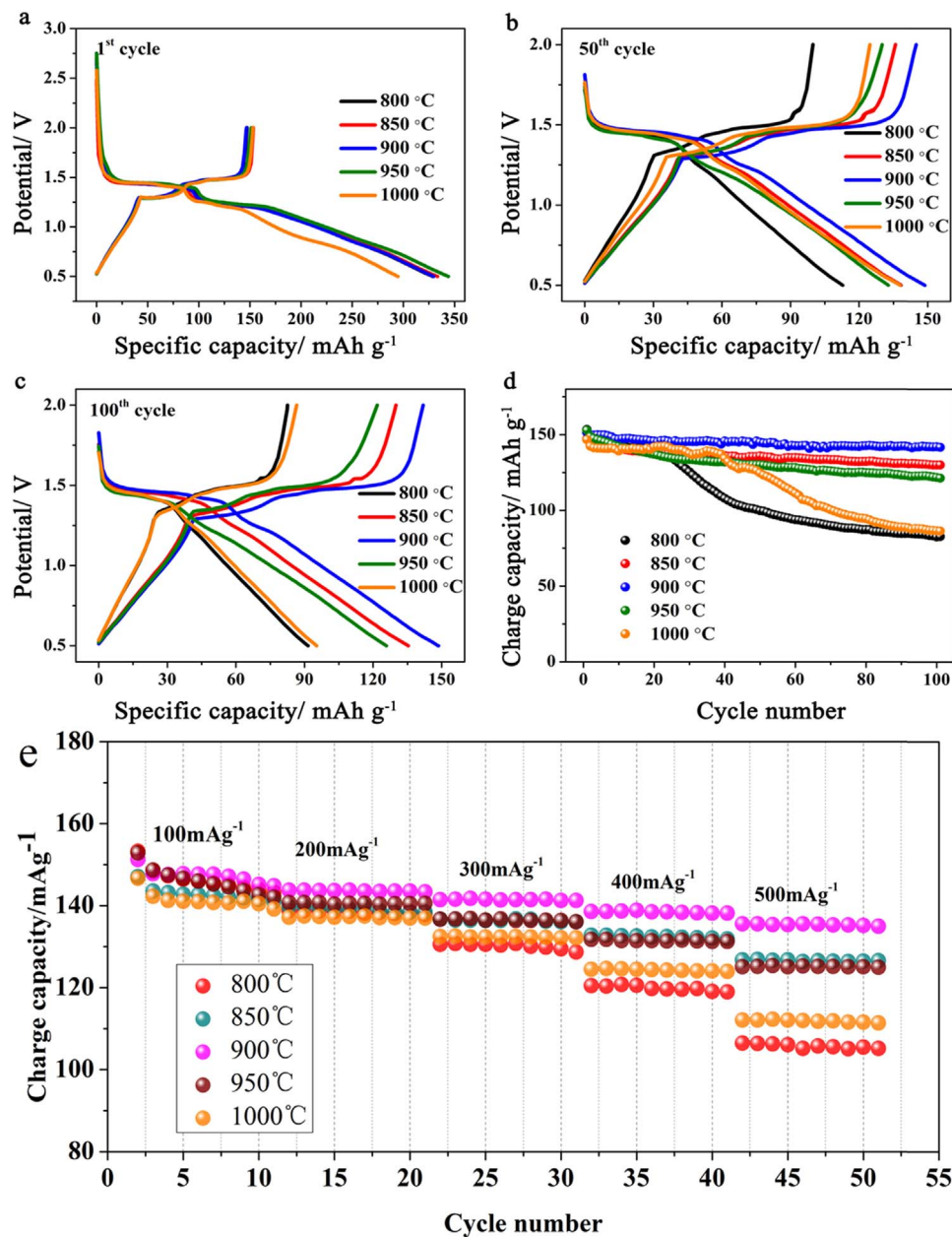


Fig. 6. The (a) 1st, (b) 50th and (c) 100th charge/discharge curves. (d) Corresponding cycling performance of $\text{PbLi}_2\text{Ti}_6\text{O}_{14}$ obtained at different temperature at a rate of 100 mA h g⁻¹. (e) Rate performance at different current densities.

Warburg diffusion impedance, respectively. According to the fitting results, the solution resistances of the five samples are 2.12, 2.25, 2.35, 3.02 and 3.32 Ω , and the charge transfer resistances are 11.29, 16.8, 18.58, 20.50 and 24.48 Ω , respectively. These results indicate that $\text{PbLi}_2\text{Ti}_6\text{O}_{14}$ calcined at 800 °C has the smallest resistance. This is attributed to the fact that the diffusion of lithium ion in the spherical particle is proportional to the particle size of the particle. The result also shows that the smaller particle of $\text{PbLi}_2\text{Ti}_6\text{O}_{14}$ has smaller internal resistance and higher lithium ion diffusion coefficient [24]. In addition, the lithium ion diffusion coefficient can be calculated by the following equation:

$$D = \frac{R^2 T^2}{2A^2 n^4 F^4 C^2 \sigma^2} \quad (1)$$

In the above equation, σ , R , T , A , n , F and C are the Warburg factors, the gas constant, the absolute temperature, the electrode surface area, the number of electrons transferred in the half reaction, the Faraday constant and the lithium ion molar concentration, respectively [25]. The relationship between Z' and the Warburg parameter σ can be expressed as follows:

$$Z' = R_e + R_{ct} + \sigma \omega^{-1/2} \quad (2)$$

The relationship between Z' and $\omega^{-1/2}$ is shown in Fig. 7c. The

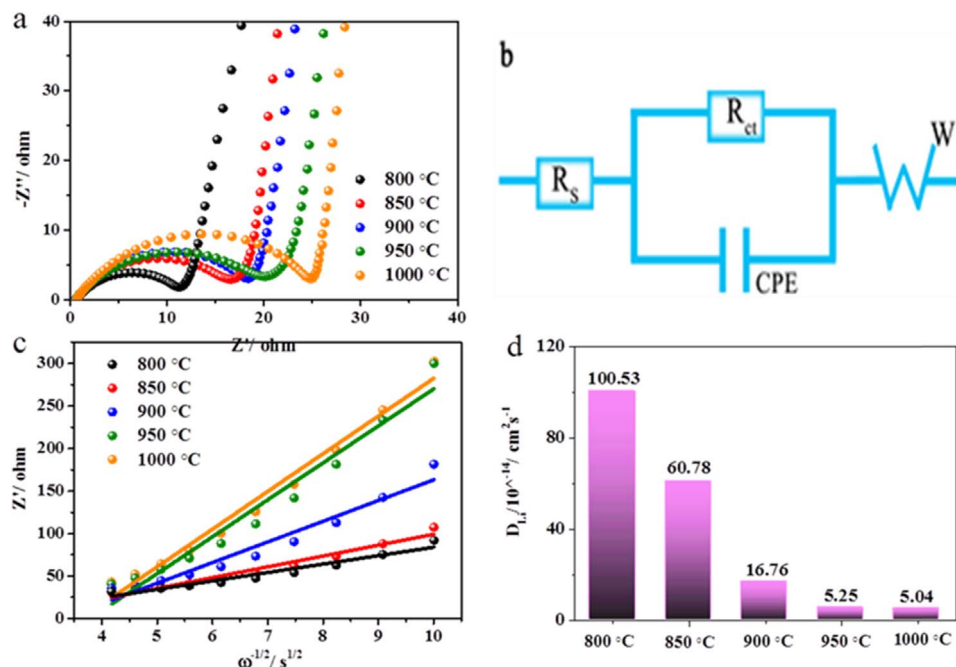


Fig. 7. (a) EIS curves of $\text{PbLi}_2\text{Ti}_6\text{O}_{14}$ obtained at different temperature. (b) The fitted equivalent circuit. (c) The relationship between Z' and $\omega^{-0.5}$ in low frequency region. (d) Lithium diffusion coefficient of $\text{PbLi}_2\text{Ti}_6\text{O}_{14}$ obtained at different calcining temperature.

calculated diffusion coefficients of lithium ions for the samples yielded at 800, 850, 900, 950 and 1000 °C are 100.53×10^{-14} , 60.78×10^{-14} , 16.76×10^{-14} , 5.25×10^{-14} and $5.04 \times 10^{-14} \text{ cm}^2 \text{ s}^{-1}$, respectively, as shown in Fig. 7d. The $\text{PbLi}_2\text{Ti}_6\text{O}_{14}$ obtained at 800 °C has the largest lithium-ion diffusion coefficient due to its smallest particle size. At the same times, the sample calcined at 900 °C has higher lithium ion diffusion coefficient than the other two samples obtained at 950 and 1000 °C.

Base on the above analysis, it can be observed that calcination temperature can affect the particle size, surface morphology, purity of $\text{PbLi}_2\text{Ti}_6\text{O}_{14}$ and thus affects the electrochemical performance. In addition, when the calcination temperature is 900 °C, $\text{PbLi}_2\text{Ti}_6\text{O}_{14}$ shows the best electrochemical performance among all the samples. Hence, 900 °C can be the most suitable calcination temperature for $\text{PbLi}_2\text{Ti}_6\text{O}_{14}$. Further study of the lithium ion insertion/extraction behaviors in $\text{PbLi}_2\text{Ti}_6\text{O}_{14}$ is shown in Fig. 8. All the diffraction peaks displaying the periodical changes during cycling illustrates that $\text{PbLi}_2\text{Ti}_6\text{O}_{14}$ has superior stability and excellent electrochemical reversibility (Fig. 8a) [25]. Based on refined data, it is known that $\text{PbLi}_2\text{Ti}_6\text{O}_{14}$ experiences a maximum change of unit volume from 2138.6 to 2167.6 \AA^3 during the whole insertion/extraction process. Fig. 8b-g elaborates the selected in-situ XRD patterns and intensity evolutions of $\text{PbLi}_2\text{Ti}_6\text{O}_{14}$. With a close observation, it is clear that the diffraction peaks (220 and 312) at 19.3° and 23.6° reduce slowly with the discharge process and the Bragg positions of these two peaks are moving [10]. During the charge process, the relative intensities and the Bragg position of these two peaks are back to the original state. Besides, the peak (221) at 20.6° completely disappears during the discharge process, while reappears at charge process. The intensity evolutions of

these diffraction peaks are also exhibited in Figs. 8c and 8f. The diffraction peaks (132, 331 and 004) at 29.1° , 30.0° and 31.0° also experience a process from debility to enhancement during charge/discharge process. The diffraction position of the peak (512) at 31.9° shifts towards low angle during the discharge process and returns to its original position during the charge process. The diffraction peaks (204 and 240) at 33.0 and 34.0° merge into a new diffraction peak during the discharge process. This peak appears at 32.9° at the end of discharge and then divides into two original peaks during the charge process. All these above results illustrate that $\text{PbLi}_2\text{Ti}_6\text{O}_{14}$ has excellent structural stability and reversibility.

4. Conclusions

To summarize, $\text{PbLi}_2\text{Ti}_6\text{O}_{14}$ has been successfully synthesized by a traditional high temperature solid state method at five different calcination temperatures. Through a series of electrochemical tests and physical characterizations, it has been confirmed that the calcination temperature has great influence on the purity, morphology and electrochemical performance of $\text{PbLi}_2\text{Ti}_6\text{O}_{14}$. Meanwhile, the results indicate that $\text{PbLi}_2\text{Ti}_6\text{O}_{14}$ obtained at 900 °C expresses the best electrochemical properties among the five samples. It provides an initial charge capacity of $151.3 \text{ mA h g}^{-1}$ at 100 mA g^{-1} . And it shows a reversible capacity of $142.0 \text{ mA h g}^{-1}$ after 100 cycles with superior capacity retention of 93.85%. In-situ XRD patterns indicate $\text{PbLi}_2\text{Ti}_6\text{O}_{14}$ has excellent structural stability.

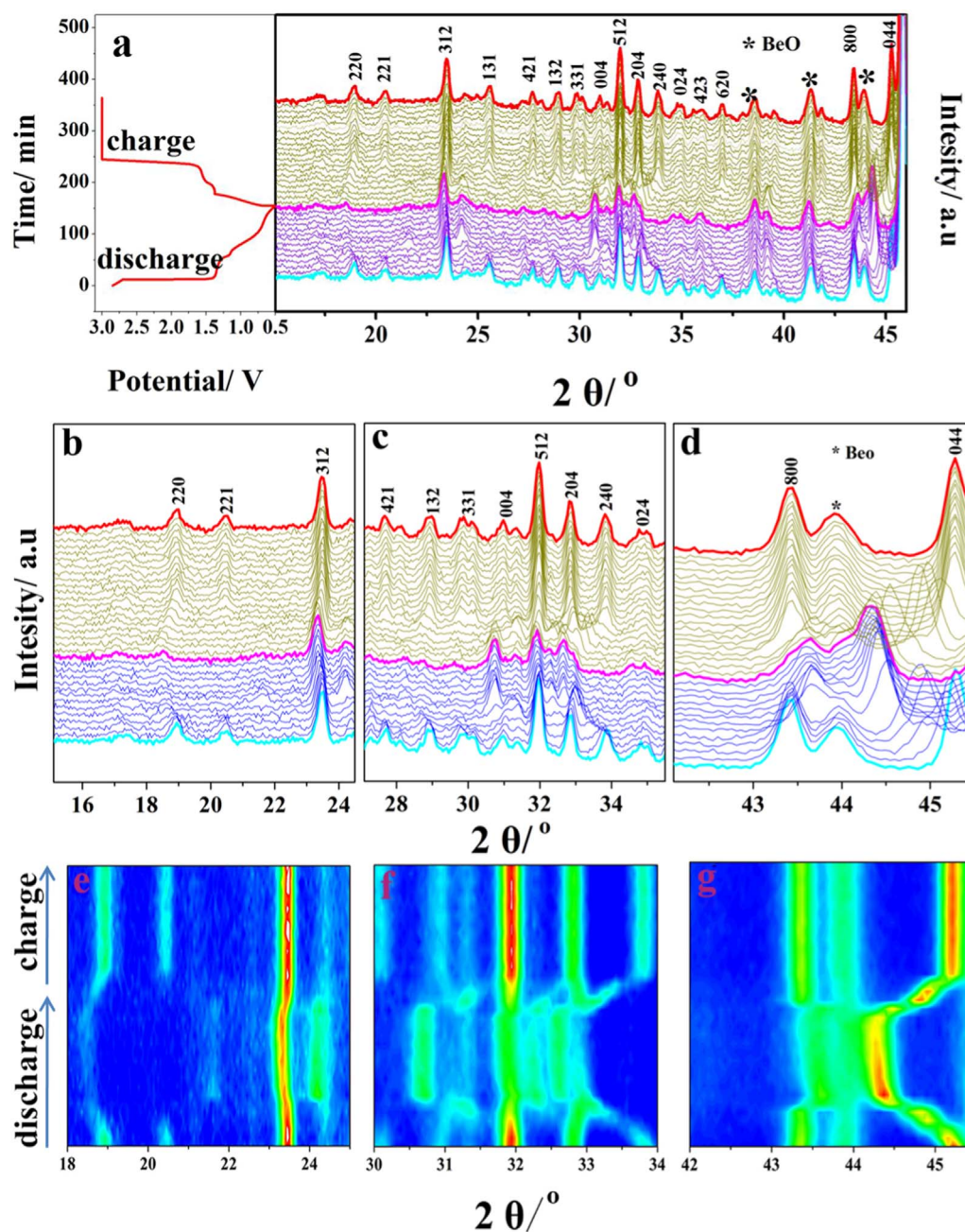


Fig. 8. (a) Overall in-situ XRD patterns during cycling. Selected in-situ XRD patterns and intensity evolutions of $\text{PbLi}_2\text{Ti}_6\text{O}_{14}$ in the 2θ range of (b) 15–24.5°, (c) 27–35.5°, (d) 41.5–45.5°, (e) 18–25°, (f) 30–34°, and (g) 42–45.5°.

Acknowledgement

This work is sponsored by National Natural Science Foundation of China (U1632114), Ningbo Key Innovation Team (2014B81005), and K.C. Wong Magna Fund in Ningbo University.

References

- [1] J. Ding, Z. Li, H.L. Wang, K. Cui, A. Kohandehghan, X.H. Tan, D. Karpuzov, D. Mitlin, Sodiation vs. lithiation phase transformations in a high rate-high stability SnO_2 in carbon nanocomposite, *J. Mater. Chem. A* 3 (2015) 7100–7111.
- [2] Y. Shi, J. Gao, H.D. Abruña, H.K. Liu, H.J. Li, J.Z. Wang, Y.P. Wu, Rapid synthesis of $\text{Li}_4\text{Ti}_5\text{O}_{12}$ /graphene composite with superior rate capability by a microwave-assisted hydrothermal method, *Nano Energy* 8 (2014) 297–304.
- [3] J.Y. Liao, X. Xiao, D. Higgins, D. Lee, F. Hassan, Z. Chen, Hierarchical $\text{Li}_4\text{Ti}_5\text{O}_{12}$ - TiO_2 composite microsphere consisting of nanocrystals for high power Li-ion batteries, *Electrochim. Acta* 108 (2013) 104–111.
- [4] J.Y. Liao, V. Chabot, M. Gu, C.M. Wang, X.C. Xiao, Z.W. Chen, Dual phase $\text{Li}_4\text{Ti}_5\text{O}_{12}$ - TiO_2 nanowire arrays as integrated anodes for high-rate lithium-ion batteries, *Nano Energy* 9 (2014) 383–391.
- [5] M. Chen, W. Li, X. Shen, G.W. Diao, Fabrication of core-shell $\alpha\text{-Fe}_2\text{O}_3$ @ $\text{Li}_4\text{Ti}_5\text{O}_{12}$ composite and its application in the lithium ion batteries, *ACS Appl. Mater. Interfaces* 6 (2014) 4514–4523.
- [6] I. Koseva, K. Lliev, P. Peshev, Regions of existence of the SrTiO_3 phase in the system $\text{SrO-TiO}_2\text{-Li}_2\text{O-B}_2\text{O}_3$, *Mater. Res. Bull.* 26 (1991) 659–666.
- [7] I. Koseva, P. Peshev, S. Pechev, P. Gravereau, J.P. Chaminade, A new strontium lithium titanium oxide, $\text{SrLi}_2\text{Ti}_6\text{O}_{14}$: crystal growth and structure determination, *Z. Naturforsch. B: Chem. Sci.* 57 (2002) 512–518.
- [8] I. Koseva, J.P. Chaminade, P. Gravereau, S. Pechev, P. Peshev, J. Etourneau, A new family of isostructural titanates, $\text{MLi}_2\text{Ti}_6\text{O}_{14}$ ($M = \text{Sr, Ba, Pb}$), *J. Alloy. Compd.* 389 (2005) 47–54.
- [9] D. Dambournet, I. Belharouak, K. Amine, $\text{MLi}_2\text{Ti}_6\text{O}_{14}$ ($M = \text{Sr, Ba, 2Na}$) lithium insertion titanate materials: a comparative study, *Inorg. Chem.* 49 (2010) 2822–2826.
- [10] P. Li, S.S. Qian, H.X. Yu, L. Yan, X.T. Lin, K. Yang, N.B. Long, M. Shui, J. Shu, $\text{PbLi}_2\text{Ti}_6\text{O}_{14}$: a novel high-rate long-life anode material for rechargeable lithium-ion batteries, *J. Power Sources* 330 (2016) 45–54.
- [11] K.Q. Wu, D.J. Wang, X.T. Lin, L.Y. Shao, M. Shui, X.X. Jiang, N.B. Long, Y.L. Ren,

- J. Shu, Comparative study of $\text{Na}_2\text{Li}_2\text{Ti}_6\text{O}_{14}$ prepared by different methods as advanced anode material for lithium-ion batteries, *J. Electroanal. Chem.* 717–718 (2014) 10–16.
- [12] H.S. Li, L.F. Shen, B. Ding, G. Pang, H. Dou, X.G. Zhang, Ultra long $\text{SrLi}_2\text{Ti}_6\text{O}_{14}$ nanowires composed of single-crystalline nanoparticles: promising candidates for high-power lithium ions batteries, *Nano Energy* 13 (2015) 18–27.
- [13] M.M. Lao, X.T. Lin, P. Li, L.Y. Shao, K.Q. Wu, M. Shui, N.B. Long, Y.L. Ren, J. Shu, Preparation and electrochemical characterization of $\text{Li}_{2+x}\text{Na}_{2-x}\text{Ti}_6\text{O}_{14}$ ($0 \leq x \leq 0.2$) as anode materials for lithium-ion batteries, *Ceram. Int.* 41 (2015) 2900–2907.
- [14] X.T. Lin, P. Li, P.F. Wang, H.X. Yu, S.S. Qian, M. Shui, X. Zheng, N.B. Long, J. Shu, $\text{SrLi}_2\text{Ti}_6\text{O}_{14}$: a probable host material for high performance lithium storage, *Electrochim. Acta* 180 (2015) 831–844.
- [15] M.M. Lao, P. Li, P.F. Wang, X. Zheng, W.J. Wu, M. Shui, X.T. Lin, N.B. Long, J. Shu, Advanced electrochemical performance of $\text{Li}_{1.95}\text{Al}_{0.05}\text{Na}_2\text{Ti}_6\text{O}_{14}$ anode material for lithium ion batteries, *Electrochim. Acta* 176 (2015) 694–704.
- [16] P.F. Wang, P. Li, T.F. Yi, X.T. Lin, H.X. Yu, Y.R. Zhu, S.S. Qian, M. Shui, J. Shu, Enhanced lithium storage capability of sodium lithium titanate via lithium-site doping, *J. Power Sources* 297 (2015) 283–294.
- [17] G. Zhang, X.D. Lou, General synthesis of multi-shelled mixed metal oxide hollow spheres with superior lithium storage properties, *Angew. Chem. Int. Ed.* 53 (2014) 9041–9044.
- [18] J. Wang, L.F. Shen, H.S. Li, X.Y. Wang, P. Nie, B. Ding, G.Y. Xu, H. Dou, X.G. Zhang, A facile one-pot synthesis of TiO_2 /nitrogen-doped reduced graphene oxide nanocomposite as anode materials for high-rate lithium-ion batteries, *Electrochim. Acta* 133 (2014) 209–216.
- [19] Z.H. Chen, I. Belharouak, Y.K. Sun, K. Amine, Titanium-based anode materials for safe lithium-ion batteries, *Adv. Funct. Mater.* 23 (2013) 959–969.
- [20] X.T. Lin, P. Li, L.Y. Shao, M. Shui, D.J. Wang, N.B. Long, Y.L. Ren, J. Shu, Lithium barium titanate: a stable lithium storage material for lithium-ion batteries, *J. Power Sources* 278 (2015) 546–554.
- [21] P.F. Wang, P. Li, T.F. Yi, X.T. Lin, Y.R. Zhu, L.Y. Shao, M. Shui, N.B. Long, J. Shu, Improved lithium storage performance of lithium sodium titanate anode by titanium site substitution with aluminum, *J. Power Sources* 293 (2015) 33–41.
- [22] M.S. Wu, H.W. Chang, Self-assembly of NiO-coated ZnO nanorod electrodes with core-shell nanostructures as anode materials for rechargeable lithium-ion batteries, *J. Phys. Chem. C* 117 (2013) 2590–2599.
- [23] R.H. Wang, C.H. Xu, J. Sun, L. Gao, H.L. Yao, Solvothermal-induced 3D macroscopic SnO_2 /nitrogen-doped graphene aerogels for high capacity and long-life lithium storage, *ACS Appl. Mater. Interfaces* 6 (2014) 3427–3436.
- [24] M.S. Song, R.H. Kim, S.W. Baek, K.S. Lee, K. Park, A. Benayad, Is $\text{Li}_4\text{Ti}_5\text{O}_{12}$ a solid-electrolyte-interphase-free electrode material in Li-Ion batteries reactivity between the $\text{Li}_4\text{Ti}_5\text{O}_{12}$ electrode and electrolyte, *J. Mater. Chem. A* 2 (2014) 631–636.
- [25] N. Mahmood, C.Z. Zhang, F. Liu, J.H. Zhu, Y.L. Hou, Hybrid of Co_3Sn_2 @Co nanoparticles and nitrogen-doped graphene as a lithium ion battery anode, *ACS Nano* 7 (2013) 10307–10318.